Journal of Oceanography (2023) 79:13–26
https://doi.org/10.1007/s10872-022-00659-0

ORIGINAL ARTICLE

Wave setup at the Minamitorishima tide gauge

Richard D. Ray[1] · **Mark A. Merrifield**[2] · **Philip L. Woodworth**[3]

Received: 9 March 2022 / Revised: 30 June 2022 / Accepted: 2 August 2022 / Published online: 17 August 2022
This is a U.S. Government work and not under copyright protection in the US; foreign copyright protection may apply 2022

Abstract
A tide gauge situated on the western shore of Minamitorishima, a small atoll in the western Pacific, has measured sea levels significantly impacted by wave setup. Evidence for this rests with (a) strong correlations between sea level anomalies and high swell and (b) sea-level differences with satellite altimetry that display near-linear dependence on offshore swell heights (regression coefficient 30 cm per meter of swell). Setup is primarily induced by swell from the northwest. We develop models of wave setup which lead to corrected sea levels better reflecting the surrounding ocean, and thus more readily useful to studies of regional sea level and practical applications such as altimetry calibration. The wave setup is also evidently affecting measurements of the tide, with suppressed tide amplitudes in winter when swell is generally largest. In February 2020 the tide gauge was relocated to the southern shore of the island, and the wave setup is now markedly reduced.

Keywords Wave setup · Sea level · Satellite altimetry · Minamitorishima atoll · Seasonal variability · Seasonal tide changes

1 Introduction

Three decades ago satellite altimetry was christened "the 2-cm solution" to the sea-level problem (Cheney et al. 1994) thanks to excellent comparisons with tide-gauge measurements at small, open-ocean islands. Over the years that assessment has continued to hold up for most open-ocean islands (e.g., Mitchum 1998; Ray et al. 2010; Vinogradov and Ponte 2011). There are, of course, exceptions. One of the worst island comparisons has historically been for Minamitorishima (formerly Marcus Island), a very small atoll in the western Pacific (Fig. 1), located about 2000 km southeast of Tokyo at 24°17′N, 153°59′E. Altimeter and tide-gauge measurements there are especially discordant at the annual cycle (Vinogradov and Ponte 2010; Ray et al. 2021). Figure 2 compares an altimeter-based time series of sea level near the island with (smoothed) daily means from the island tide gauge—see Appendix A for the methodology—and the large discrepancies in the two-time series are evident. The time series of differences (lower panel) has a root-mean-square (rms) of 13.5 cm, far above the "2-cm solution." There are many possible reasons for poor agreement between an island tide gauge and altimetry (e.g., Williams and Hughes 2013), but recent work has attributed the poor agreement at Minamitorishima to effects of wave setup on the island (Ray et al. 2021). A primary purpose of the present paper is to explore in more detail the setup effect there, including its possible change after a recent relocation of the tide gauge on the island.

Wave setup occurs when breaking waves cause an increase in time-averaged (nominally longer than 30 min) water level within and shoreward of the surf zone (Woodworth 2019). Breaking waves transfer momentum to the water column which, in steady state, is balanced by a cross-shore sea level gradient resulting in increased water levels at the shoreline (Longuet-Higgins and Stewart 1962). Setup has been well documented along island shorelines (Munk and Sargent 1948), harbors (Woodworth 2020), and lagoons (Aucan et al. 2012). At island shorelines protected by a fringing reef, with a shallow reef flat that extends to the shoreline, wave breaking at the outer reef edge effectively dissipates incident wave energy (Monismith 2007),

✉ Richard D. Ray
richard.ray@nasa.gov

Mark A. Merrifield
mamerrifield@ucsd.edu

Philip L. Woodworth
plw@noc.ac.uk

[1] NASA Goddard Space Flight Center, Greenbelt, MD, USA

[2] Scripps Institution of Oceanography, University of California, San Diego, La Jolla, CA, USA

[3] National Oceanography Centre, Joseph Proudman Building, Liverpool, UK

Fig. 1 Image of Minamitorishima (24°17′N, 153°59′E). Red circles mark the approximate locations of the tide gauge: (1) before February 2020 and (2) after February 2020. Wave setup is pronounced at the first location. Note lack of apparent reef along most of the southern coast

leaving setup (Gourlay 1996; Vetter et al. 2010) and infragravity waves (Pomeroy et al. 2012; Becker et al. 2014) as the dominant wave-driven shoreline response. Wave setup tends to be the dominant nontidal contributor to total water levels, contributing significantly to island flooding during energetic wave events (Hoeke et al. 2013; Merrifield et al. 2014; Cheriton et al. 2016). Below we explore some aspects of wave setup at Minamitorishima, using sea level measurements from the tide gauge and from satellite altimetry, and wave information from a reanalysis model.

Information about the Minamitorishima tide gauge is briefly reviewed in Sect. 2. In Sect. 3 the satellite altimetry is used to remove the regional oceanographic signal from the tide gauge measurements, which allows us to better isolate the local signal from setup. Dependence on wind waves versus swell is compared. Even without removing altimetry, however, the tide gauge data reveal relatively high-frequency anomalies associated with the wave field; these are highlighted in Sect. 4. Two setup models are developed in Sect. 5 and used to revisit Fig. 2, with much-improved agreement between the tide gauge and altimeter sea levels. These models address a second purpose of our work here: to develop an adjustment of the Minamitorishima tide gauge data that allows the measurements to reflect more accurately the regional sea level. Finally, on a related but somewhat tangential topic, Sect. 6 explores some unusual perturbations of the measured tide at the island caused by the wave setup effects.

2 Tide gauge at Minamitorishima

Tide gauge measurements at the atoll have been collected by the Japan Meteorological Agency (JMA) and are available in the major international archives starting with the year 1997. Information available from the Intergovernmental

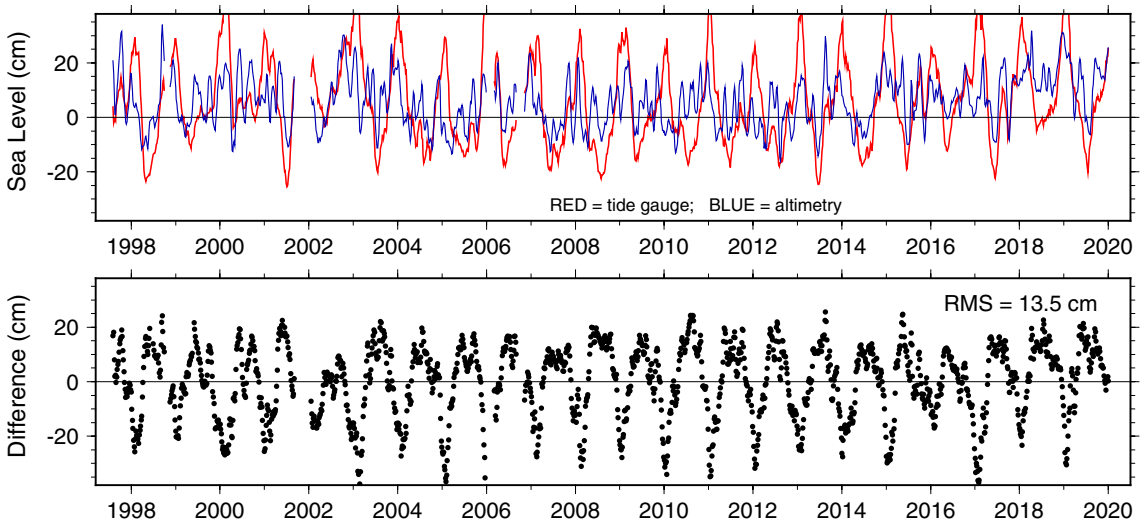

Fig. 2 (Top) Comparison of altimetric sea level measurements (from DUACS DT-2018; Taburet et al. (2019)) with daily mean sea levels from the Minamitorishima tide gauge (adjusted as described in Appendix A and smoothed to match approximately the temporal smoothing in the gridded altimetry). Relative bias is arbitrary. (Bottom) Difference in the sense altimeter minus tide gauge

Oceanographic Commission notes the gauge is a pressure sensor with 1-minute sampling, although in this work we used hourly and daily mean data from the University of Hawaii Sea Level Center.

Useful additional information has been kindly provided to us by the JMA Atmospheric Environment and Ocean Division. They confirm the gauge is a pressure instrument, with auxiliary measurements of atmospheric pressure also collected to ensure the gauge is reporting sea level only. Moreover, they report that the tide gauge, previously located on the western shore of the island, was moved after February 2020 to the southern shore. The older gauge coordinates are (24.2911°N, 153.9775°E); the new coordinates are (24.2822°N, 153.9783°E). The gauge relocation plays an important role in our analysis below. As Fig. 1 indicates, a reef with breaking waves is readily apparent on the west side, but the reef appears mostly absent on the south side.

3 Sea levels, wind waves, and swell

Building on and extending recent work (Ray et al. 2021), this section lays out evidence that the differences between altimeter and tide gauge sea levels at Minamitorishima are dominated by wave effects. We again examined sea-level differences with altimetry, similar to Fig. 2 but now with unsmoothed daily means from the tide gauge, with a goal to discover how these differences are affected by the wave environment. In this context, gridded DUACS altimetry, with an inherent temporal smoothing of roughly 30 days (see Appendix A), is used to remove the regional low-frequency oceanographic variability from the tide-gauge record. Information about the wave environment was extracted from the European Centre for Medium-Range Weather Forecasts ERA5 reanalysis (Hersbach 2020); these are hourly data on a 0.25° global grid. Taking a grid point near the island, we formed daily means of ERA5 wave heights and wave directions, which were matched up with the daily sea levels.

Critical for our application, the ERA5 wave data have been decomposed into wind waves (or windsea) and swell. Their two-dimensional wave spectra are decomposed according to whether spectral components are, or are not, considered to be subject to local wind forcing. This partitioning is dependent upon wind stress, linear-wave phase speed, and the relative directions between wind and waves; see Bidlot (2016) for details. In the following, wave direction refers to the direction, clockwise from north, from which the waves are propagating; thus, 90° refers to westward propagating waves, i.e., coming from the east.

Figure 3 shows sea-level differences (in the sense tide gauge minus altimeter) as a function of significant wave height, color coded by wave direction, for both wind waves and swell. In each panel is a small "Rose diagram," essentially a histogram showing the relative number of waves coming from each direction. Reflecting the predominant easterly winds at this location, most wind waves are arriving from the east. The swell is also predominantly from the east, but with a significant fraction also from the north and northwest.

The swell-wave diagram of Fig. 3 shows the tell-tale pattern of wave setup, with large waves correlated with large sea level anomalies at the tide gauge, in a quasi-linear relationship. The pattern is most pronounced for swell arriving from the northwest. With the tide gauge sitting

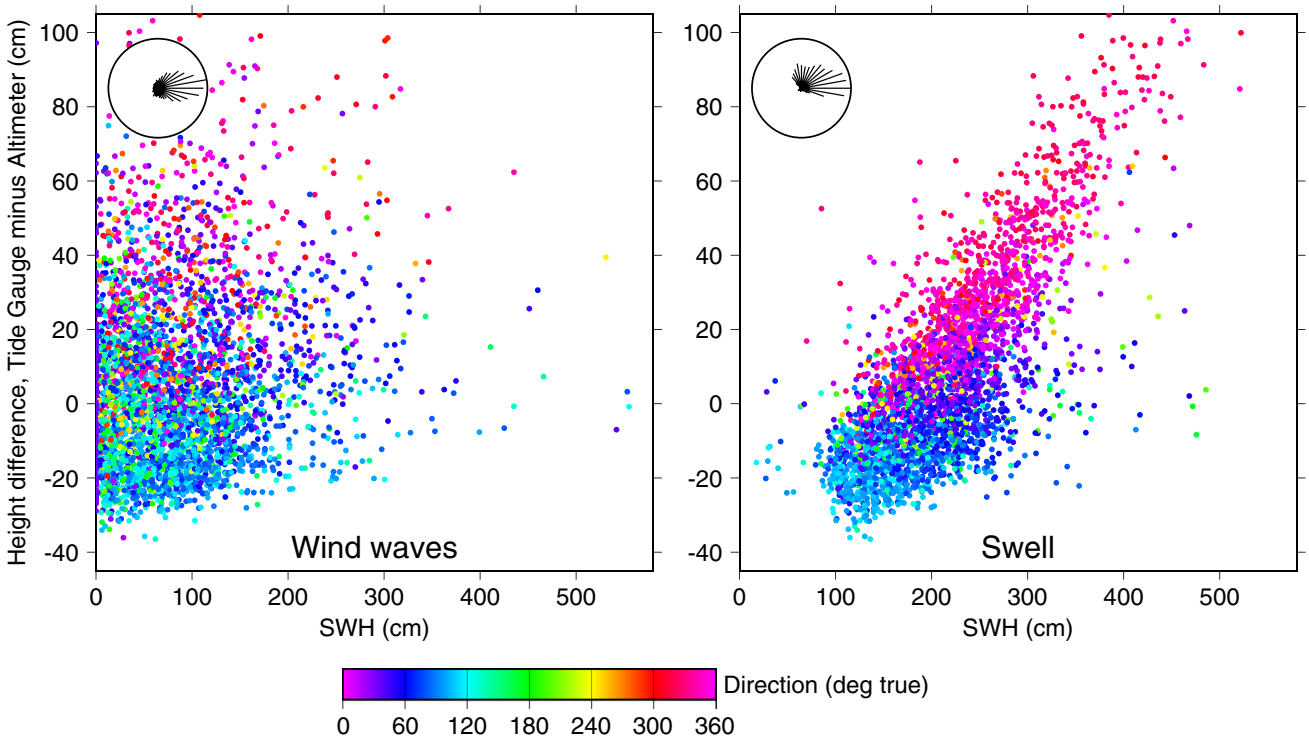

Fig. 3 Sea level differences between daily mean heights at the Minamitorishima tide gauge and gridded DUACS altimeter data, shown as a function of significant wave height for (left) wind waves and (right) swell waves. Each daily height difference is color-coded according to the wave direction. The large wave setup effect is seen to be from swell, mostly arriving from the northwest. Small Rose diagrams in the upper left indicate most waves at Minamitorishima arrive from the east, but a significant fraction of swell is from the north and northwest. Wave data are from ERA5 reanalysis. These data are for the time period 2002–2018, thus excluding data after the tide gauge was relocated in early 2020

on the western side of the island, it is situated directly in the face of northwesterly swell breaking at the reef, so the dependence on wave direction seen in Fig. 3 is as expected.

Examining only the swell arriving from the northwest, i.e., falling in the wave-direction quadrant [270°, 360°], and assuming a linear relationship between sea level and offshore wave heights, we obtained an estimated regression slope of 30.3 ± 0.4 cm m^{-1}. That is, a 1-meter swell from the northwest induces a 30 cm setup. This slope estimate is based on an orthogonal regression method, which allows for errors in both dependent and independent variables. In any given environment, wave setup is a complicated function of bottom topography, reef geometry, and incident wave field, but a setup of 30% of offshore wave height falls well within the range of reported in situ investigations (e.g., Vetter et al. 2010; Dodet et al. 2019).

In contrast to the swell waves, the wind waves in Fig. 3 show no obvious pattern, aside from a suggestion that the largest sea level anomalies appear to coincide with the relatively few wind waves arriving from the northwest. There is no evident dependence of sea level on wave height, as there is for the swell.

For many coastal tide gauges there could be a similar dependence on the wind (wind setup). However, for an island as small as Minamitorishima, one expects little wind setup because there is so little coastline against which a significant setup can develop. A diagram similar to Fig. 3 (not shown) does suggest a possible, weak, relationship with winds, as the largest sea level anomalies are associated with winds from the northwest, rather similar to the wind waves of Fig. 3. We briefly revisit this point below.

It should be mentioned that dependence of sea-level differences on wave height, as in Fig. 3, can also arise from sea-state bias errors in altimeter measurements. Such bias errors can arise from a combination of effects, but generally the largest is an electromagnetic bias caused by radar return power from wave troughs exceeding that returned from wave crests, resulting in altimetric height estimates biased too low (e.g., Walsh et al. 1989). The proportionality constant for sea-state bias, however, is an order of magnitude smaller than that observed here. For example, in the DUACS processing, the sea-state bias correction for TOPEX altimetry is based on a non-parametric model of Tran et al. (2010), which for a typical wave height of 2 m equals approximately 7 cm, or 3.5%.

That model, of course, cannot be perfect, so there may be a very small possible contribution to our estimate of wave setup owing to errors in sea-state bias. However, we can safely rule out all but a very minor contribution, because we have examined a number of other island tide gauges in the manner of Fig. 3 and for the majority we find no dependence on wave height at all.

4 Variability of sea level and swell

Simple time series comparisons of sea level and offshore wave heights can also further establish an evident relationship between the two; see, for example, recent work by Woodworth (2020) who studied wave setup at Tristan de Cunha in the South Atlantic. A display of the sea-level and wave data over several years sheds useful light on the variability of each as well as their co-variability.

Figure 4 shows the daily mean sea levels at Minamitorishima and the swell significant wave heights, the latter color-coded according to the swell direction. The largest swell generally appears in winter, beginning around mid-December each year and extending into February (as in 2019) or beyond (notably 2017). In keeping with the statistics of Sect. 3, these large wintertime waves are predominantly from the northwest. Occasional appearances of large swell in summer are mostly from the south. The correlation of large swell with large sea-level anomalies is visually striking, but only when the waves are arriving from the north or northwest. Large waves from the south have a much smaller, if any, effect on sea level (at the scale of the figure). A clear example occurs in August 2016 when waves during the beginning of the month have only a small sea-level effect, but once the swell begins arriving from the north at the end of August the sea-level effect is several times more pronounced, even though the waves are slightly smaller.

The other striking feature of Fig. 4 is the sharp reduction in sea-level variability once the tide gauge is relocated in early 2020. Once that happens, the tide gauge is sheltered from the northwesterly swell and the large waves during April 2020 evidently had little effect on sea level. Unfortunately, there were no available tide-gauge data between December 2020 and mid-March 2021, and the data were gappy in late 2021, so we have yet to observe the new sea-level response during wintertime conditions. Nonetheless, occurrences of swell from due south during the summer of 2021 are seen to have no obvious sea-level response at the new location. This suggests that the large wave setup at the Minamitorishima tide gauge is no longer occurring. We await further wintertime observations to confirm this.

5 Models of wave setup

In this section, two models are developed for wave setup at Minamitorishima, both relevant to the tide gauge location on the western shore before the relocation. One goal is to develop a model to remove wave effects to obtain a more accurate measure of the surrounding sea level. The first model is purely empirical; the second semi-analytic. In both cases we used data only from before February 2020 to constrain model parameters.

5.1 Empirical model

Figure 3 shows the evident setup relationship between sea-level anomalies and offshore ocean swell. Figure 5a shows the same data but refashioned to show sea-level anomalies as a two-dimensional function of swell height and direction. An empirical, non-parametric model of setup at this location can be constructed from these data in straightforward manner.

We analyzed the data of Fig. 5a in (overlapping) direction bands and used simple linear regression to fit observed sea-level anomalies to swell height. After slight two-dimensional smoothing, the result is shown in Fig. 5b. The regression fits can safely interpolate across regions of no data, but we avoided extrapolation in certain directions where no large waves had ever been observed; those regions are left blank in the figure. The individual regression slope estimates are shown in Fig. 6. The slopes are seen to vary from a maximum of 30 cm m^{-1} for wave directions near the peak at 308°, to a low of 4 cm m^{-1} for directions in the 150°–200° band. The latter, if we allow for the uncertainty envelope, is near zero, implying little or no setup from those directions.

The slope estimates of Fig. 6 are seen to fall off rapidly from the peak direction of 308°, with a possible functional form depending on $\cos(\theta - 308°)$. Based on physical grounds—see Eq. (2) below—that function may be expected to be proportional to $[\cos(\theta - 308°)]^{2/5}$. For the data in Fig. 6, however, we find the (2/5) exponent gives a falloff slightly too slow, and a better fit is obtained with exponent (1/2). The fit is shown as the dotted line in the figure for the section of data where the cosine is positive.

Since the model is empirical, it is unsurprising that using it to remove wave setup from the tide gauge data significantly reduces the mismatch with altimetry that had been seen in Fig. 2. The revised data are shown in Fig. 7. The original rms difference between the tide gauge and altimeter was 13.5 cm, and this is now reduced to 4.8 cm. This value is still larger than the canonical 2 cm of Cheney et al. (1994), but it is small enough to be used with some confidence in applications that assume the tide gauge is measuring open-ocean sea level.

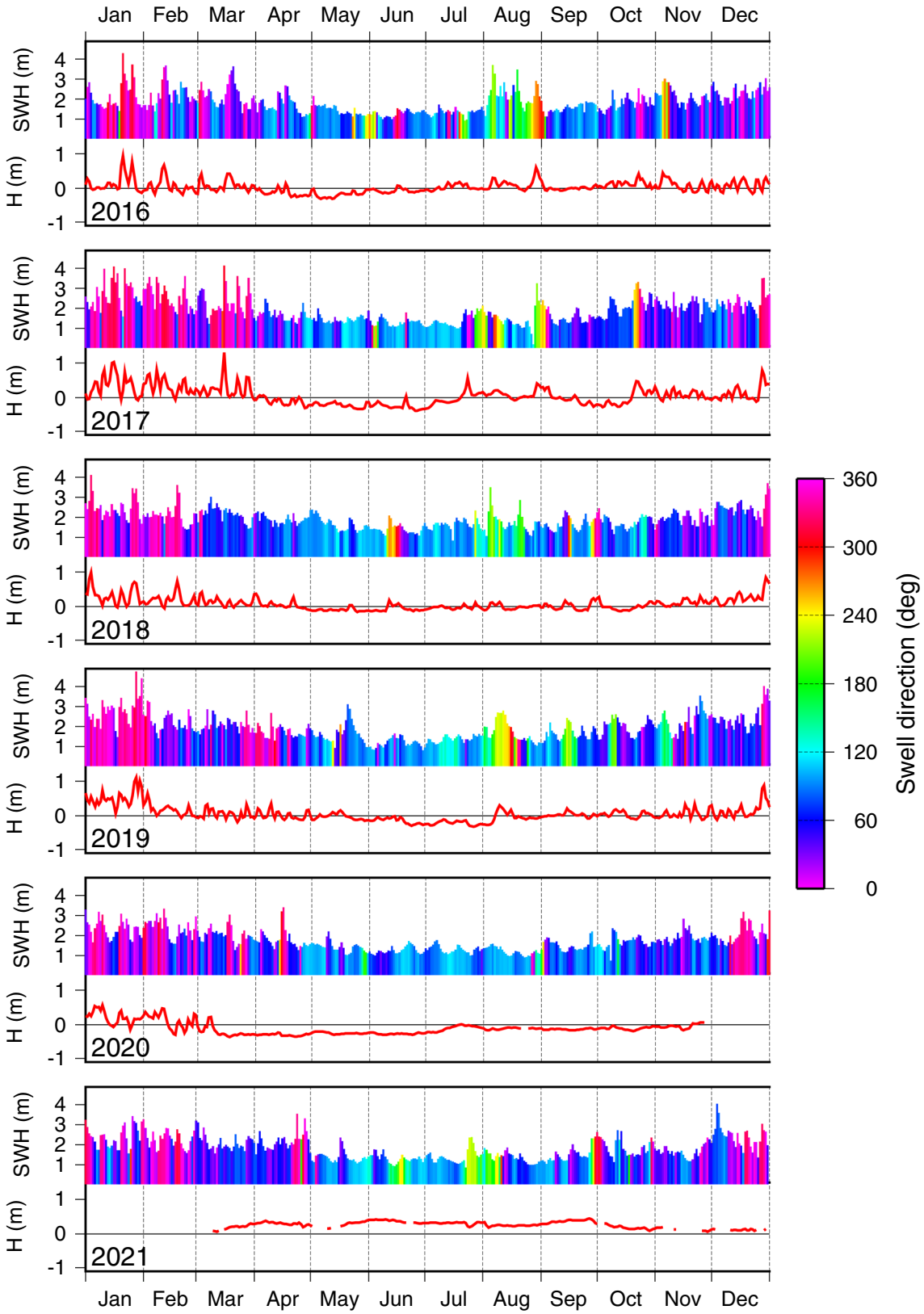

Fig. 4 Daily mean observations of sea level (red curves) and offshore swell significant wave height color-coded according to wave direction, shown for years 2016 through 2021. Most high-frequency sea level anomalies are seen to correlate with large wave heights, but only for waves arriving from the northwest or north (or approximate directions 270°–360°). The tide gauge was relocated from the western to the southern coast of the island in February 2020, and afterwards the wave setup effect essentially disappears

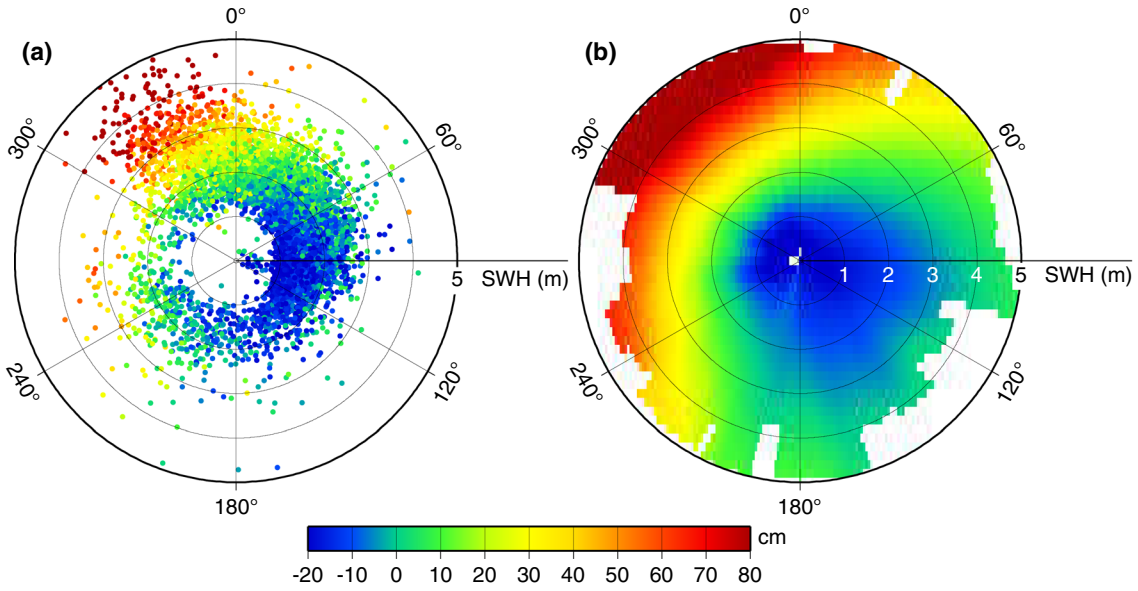

Fig. 5 **a** Color-coded sea-level differences between tide gauge and altimetry plotted as a function of swell wave height and direction. Each point represents one daily observation. The zero level for the sea level is arbitrarily set so that the mean sea-level difference is zero. **b** Gridded and smoothed version of the data in panel **a**. This two-dimensional function of swell height and direction can act as an empirical model of wave setup at the tide gauge

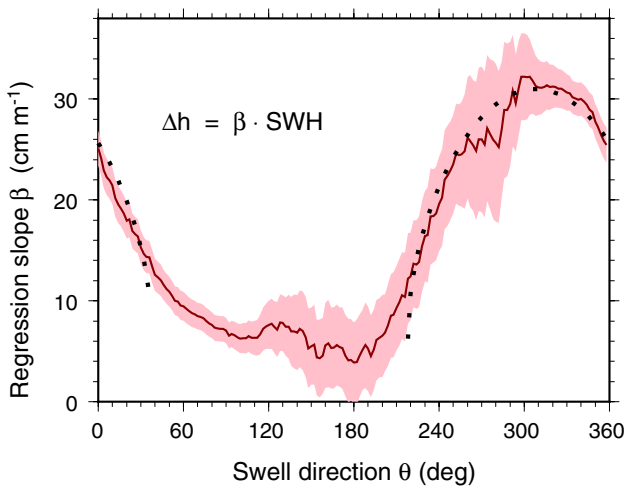

Fig. 6 Estimated linear relationship between setup anomalies and significant wave height (SWH) of swell, based on the data shown in Fig. 5a. Shaded background marks uncertainties in the slope estimates; they have been roughly scaled to account for serial correlation in the data, based on the autocorrelation (approximately 0.83) of the entire daily tide gauge series. The dotted line represents a functional dependence on direction θ according to $[\cos(\theta - 308°)]^{1/2}$, valid only where the cosine is positive. This functional form follows Eq. (2), but here with a slightly larger exponential (1/2 rather than 2/5)

In particular, the annual cycle in sea level is now consistent between tide gauge and altimetry, once the annual cycle in setup is added to the open-ocean (altimeter) component; see Fig. 8, where the "setup" vector is based on solving for an annual cycle in a time series from our empirical setup model.[1] The good agreement now closes a large discrepancy in measurements of the annual cycle between the island gauge and satellite altimetry, first noted by Vinogradov and Ponte (2010).

5.2 Semi-analytical model

As an alternative to a purely empirical approach, we also examined a semi-analytical model previously used with some success to study setup-induced water-level extremes (Merrifield et al. 2014). The gauge-altimeter differences are still used to solve a regression equation on wave height, with those differences used as a proxy for setup η:

$$\eta = \beta_1 H_b + \beta_0. \tag{1}$$

In this case, however, the wave height H_b is of the breaking waves on the reef face. An expression for breaking wave height H_b based on offshore wave parameters can be obtained by invoking conservation of wave energy flux,

[1] We have confirmed that the phase of wave setup obtained here using our empirical model is consistent with the presumed annual cycle of infragravity wave energy at the atoll. The latter was estimated by computing the rms of 1-minute sea levels within 4-hour windows using three years of data from the MISELA dataset (Zemunik et al. 2021), detided and high-pass filtered with a 2-hour cutoff.

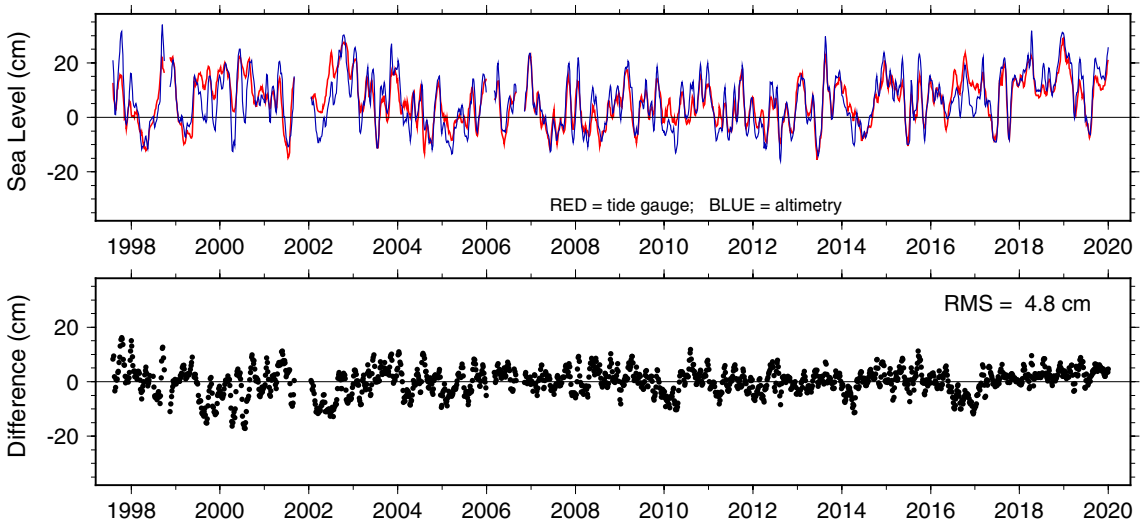

Fig. 7 Similar to Fig. 2 but after the tide gauge data have been adjusted for wave setup using the empirically-based two-dimensional model of Fig. 5b. The rms of the altimeter and tide gauge differences is now 4.5 cm, much lower than the original 13.5 cm. The differences in the lower panel are in the sense altimeter minus tide gauge

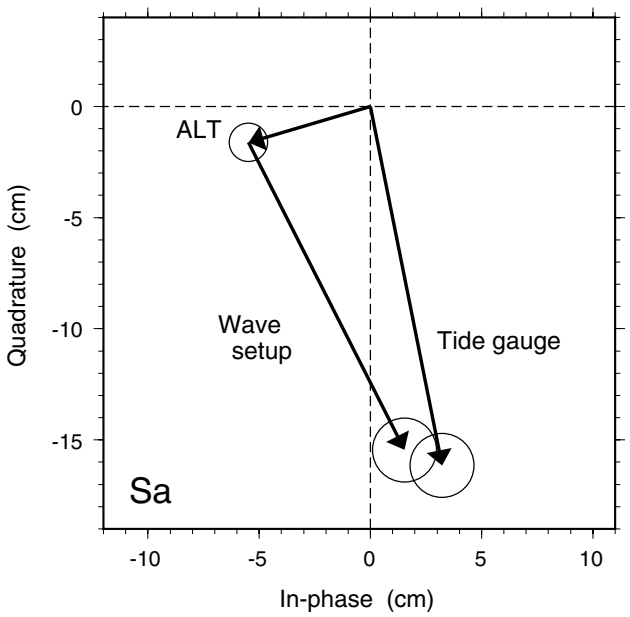

Fig. 8 Annual cycle of sea level, showing closure between tide gauge measurement (pre-2020) and altimetry after addition of the wave-setup component. The latter is based on solving for an annual cycle in a time series of the empirical setup model (Sect. 5.1). For this figure, the previously removed gravitational tide, pole tide, and inverted barometer have been restored to the altimeter data. Phase of annual cycle is relative to the spring equinox, following tidal conventions (thus, a phase near 280°, as is the case here for the tide-gauge data, peaks approximately near the beginning of the calendar year). Updated from Ray et al. (2021) with our improved setup model

assumed to be shore-normal at breaking, and relating the wave height to water depth at breaking, $H_b = \gamma h_b$, yielding

$$H_b = \left[H_0^2 T_0 (4\pi)^{-1} \cos(\theta_0 - \theta_N) \sqrt{(\gamma g)}\right]^{2/5} \quad (2)$$

with H_0, T_0, θ_0 being the significant wave height, mean period, and mean direction of the deep-water swell as extracted from ERA5 fields (cf. Monismith et al. 2013). The shore-normal angle θ_N was set to 308°, based on Fig. 6. The scalar γ (Raubenheimer et al. 1996) varies with the tide and was found by Merrifield et al. (2014) to lie generally in the range 1.1–1.3; we here set γ to a constant 1.2. Owing to the fractional exponential, Eq. (2) is applicable only to wave conditions satisfying $\cos(\theta_0 - \theta_N) > 0$. That restriction removes the great majority of waves arriving at the island (see Rose diagram in Fig. 3), but those waves are responsible for little setup, as seen above.

Over the period 1997–2019 there are 7821 daily tide-gauge and altimeter differences, of which 2716 (or 35%) remain after the restriction on wave direction. From these daily differences, least-squares estimation yields $\beta_1 = 20 \pm 1$ cm m^{-1}; orthogonal regression yields a nearly identical result. (This β_1 coefficient is much smaller than that found in the previous section, but here the regression is on the wave field H_b rather than H_0. The estimate of β_0 is irrelevant since it depends on the arbitrarily adopted mean of the altimeter-gauge differences.)

How well each setup model fits the tide-gauge and altimeter differences is shown in Fig. 9. The empirical setup model must be expected to fit much better since it has many more free parameters. Nonetheless, the semi-analytic model is not substantially worse, with rms difference of 11.0 versus 9.1

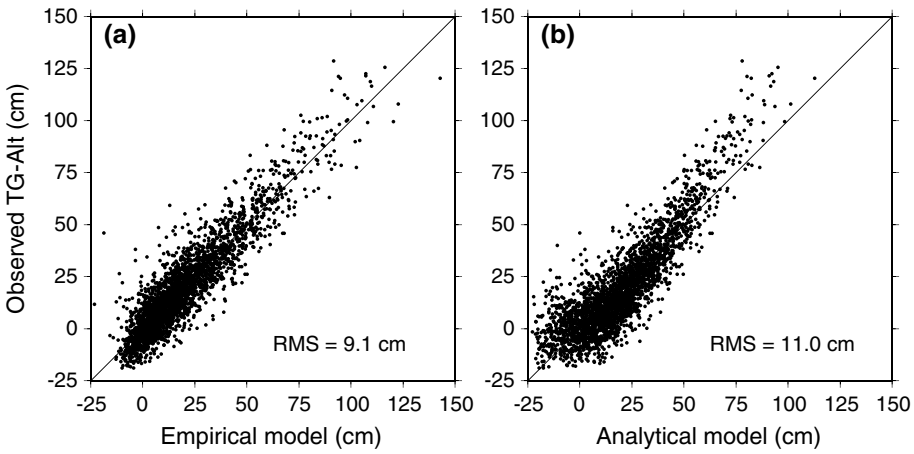

Fig. 9 Scatter diagrams of predicted wave setup versus observed daily tide-gauge/altimeter sea-level differences, based on **a** the empirical model of Sect. 5.1 and **b** the semi-analytic model of Sect. 5.2. Both panels are limited to swell directions within 90°of 308°, because model **b** is applicable only in that range.

cm. Note that both numbers are far greater than the 4.8 cm shown in Fig. 7, but they are not comparable data—Fig. 7 is based on tide gauge data low-pass filtered to match the temporal scales in the gridded altimetry; in contrast, the data in Fig. 9 are unfiltered, as both setup models were developed to apply at all frequencies, including the relatively high-frequency setup events apparent in Fig. 4.

As noted above, we anticipate little wind setup effect on this small island, but as a rough check we correlated the residuals of the semi-analytic model (Fig. 9b) with the component of the ECMWF winds in the direction of 308°. The correlation coefficient was small (0.07), implying that either (a) wind setup is very small or (b) it is subsumed into the wave setup to the extent that the northwest wind is correlated with swell.

In the remainder of this paper, we employ the empirical setup model, primarily because it gives a predicted setup for all wave conditions, not limited by direction.

6 Wave setup and the observed tide

Becker et al. (2014) studied wave setup on three coral atolls in the western Pacific (Majuro, Roi-Namur, and Kwajalein) by obtaining a series of in situ pressure and current measurements along profiles, extending from seaward of the reef, across the reef flat, and to the shore. They found wave setup depended on the tidal elevation at the reef, in the sense that their setup regression coefficient (between setup and wave height at the reef) decreased as tidal water level increased. Earlier studies have similarly reported setup dependence on tide levels (e.g., Holman and Sallenger 1985; Lugo-Fernández et al. 1998). Note that our analytical model ignored tidal elevations, although the effect formally could be incorporated into the parameter γ of Eq. (2).

This kind of tide dependence has the interesting implication that, for a given offshore wave field, the wave setup measured at the shore will have variability at tidal periods. Thus, as the wave field changes, the tide gauge seemingly measures a perturbation in the ocean tide, whereas actually it may be measuring merely a tidal perturbation in the setup. If this process occurs, the reported tide will generally have a smaller amplitude than the "true" tide offshore, with greater reduction during times of greater swell. In this section we lay out suggestive evidence that this tidal effect has been occurring at Minamitorishima (again, when the gauge was located on the western shore).

At Minamitorishima the ocean tide is relatively small: the largest constituents (pre-2020 data) are K_1 (mean amplitude 99 mm) and M_2 (mean amplitude 79 mm). Figure 10 shows monthly mean estimates of the amplitudes of both constituents, plus monthly mean estimates of sea level, all determined from hourly data over the period 1997–2019. The seasonality in tidal amplitudes is a significant fraction of the mean amplitudes. This is not the case for the tide offshore, where tides extracted from satellite altimetry, although noisy at subseasonal scales, show no strong seasonal modulation (for details see Appendix C). The tide amplitudes of Fig. 10 are seen to be very nearly mirror images of the mean sea level at the tide gauge. Since the annual cycle in sea level is known to be dominated by the annual cycle in the large wave setup (Fig. 8), the correlation between sea level and tide suggests the tide has a similar dependence on setup. That in fact would be consistent with the measurements of Becker et al. (2014). Even though those authors were observing effects during individual tidal cycles, a corollary to their observations is that the *mean* amplitude of the tide is also reduced by the continual presence of a larger wave setup. Larger setup occurs at Minamitorishima predominantly in wintertime, and this is when the tide amplitudes are evidently suppressed.

The effect can also be expressed more directly as a function of general wave setup by using our empirical model of Sect. 5, which provides an estimate of setup for every hourly tide-gauge measurement. The gauge time series can thus be partitioned according to setup, and independent

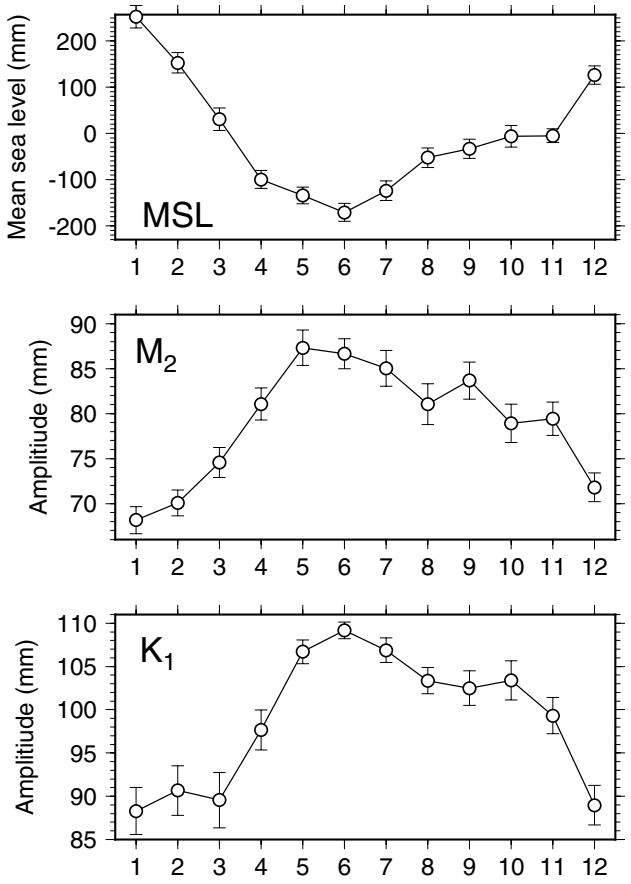

Fig. 10 Monthly mean estimates of sea level and amplitude of the M_2 and K_1 tides, showing seasonality in sea level and tidal amplitude, from data before the tide gauge was relocated in February 2020. The tide amplitudes form very nearly mirror images of the mean sea level curve. The latter reflects seasonality in swell-induced setup, as shown in Fig. 8

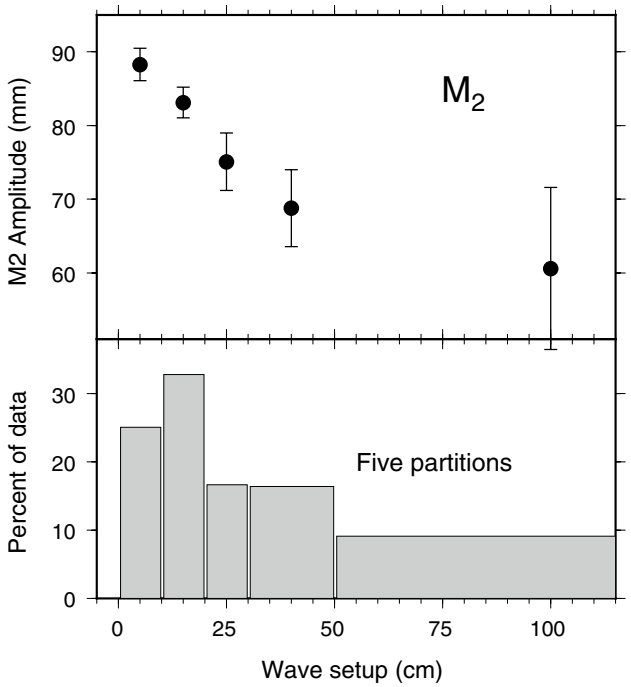

Fig. 11 Estimated amplitudes of the M_2 tide at Minamitorishima, from the western location, after breaking the hourly water-level time series into five partitions according to the wave setup at the time of each measurement and subjecting each partition to independent tidal analysis. (Wave setup was determined by using our empirical model.) Bottom panel shows percentage of data falling into each partition, with their setup bounds in cm. The estimated amplitudes of M_2 decay with increasing wave setup. We conjecture that in reality the tide gauge is observing tidal variations in wave setup, which acts to suppress the measured tide as setup increases from offshore swell

tidal analyses can be performed on each partition. The result for M_2 is shown in Fig. 11; a corresponding diagram for K_1 is qualitatively similar. It is clear that larger wave setup is coincident with smaller tide amplitudes.

Figures 10 and 11 are thus suggestive that tidal oscillations in offshore water level perturb wave setup, which appears at the tide gauge as a perturbation in the observed tide. Although this proposed explanation is consistent with the measurements obtained by Becker et al. (2014) at three other coral atolls, it is only suggestive, not proved, with the data we have in hand. For example, perhaps there is a physical mechanism whereby the real tide at the shore depends on the mean sea level shoreward of the reef; the effect might give tide estimates identical to our Fig. 10. The kind of in situ observations obtained by Becker et al. (2014) would be most welcome for resolving the issue, but the motivation for such measurements is somewhat limited now that the tide gauge has been moved to the southern shore.

For the new location, data collected so far are insufficient to determine possible seasonal tide modulations for M_2. However, early indications suggest diurnal tide amplitudes now have a significantly reduced modulation. We can report that monthly estimates of M_2 amplitudes obtained for every month since the tide-gauge relocation lie between 88 and 114 mm, with a mean value of 100 mm. Estimates of K_1 lie between 113 and 121 mm, with mean 117 mm. This indicates a systematic shift to greater amplitudes relative to those shown in Fig. 10. It is consistent with the idea of a tide, as measured at the shore, no longer being suppressed by the action of wave setup.

7 Conclusions

A pronounced wave setup at Minamitorishima was clear from a simple comparison of measured daily sea levels with offshore swell, as can be seen by the high-frequency events depicted in Fig. 4, most markedly between December and March when the swell is largest and its direction

is primarily from the north and northwest. Lacking comprehensive in situ measurements across the reef face and lagoon, of the sort obtained for example by Merrifield et al. (2014), we nonetheless could employ satellite altimetry to define offshore sea levels, which allows for better determination of the wave setup at the tide gauge, including from lower frequency variability that is not so apparent in Fig. 4. A near-linear dependence on swell height, when the direction is favorable, is striking (Fig. 3). No corresponding relationship is apparent for wind waves.

The inconsistent sea levels measured at Minamitorishima with the tide gauge and with satellite altimetry had previously been reported, with the discrepancy especially evident at the annual cycle (Vinogradov and Ponte 2010; Ray et al. 2021). Our empirical setup model—unsurprisingly since it is based on altimetry—brings the island and altimeter measurements into much better consistency (Fig. 7). The island data become a more reliable measurement of regional sea level, and could now be used with more confidence in such applications.

The setup effect at Minamitorishima has markedly changed now that the tide gauge has been relocated. Although we have insufficient data after February 2020 to be certain, the comparison with offshore swell (Fig. 4) already suggests very little setup. The lack of a reef several hundred meters from the southern shore, in contrast to the western shore, is undoubtedly responsible for the change. But directional differences may also play a role since the Rose diagrams of Fig. 3 suggest relatively little wave energy arrives from the south.

At the old location, the tide gauge was observing a tidal signal that was evidently affected by wave setup, with tide amplitudes suppressed during periods of larger swell. Using in situ measurements at other Pacific atolls, Becker et al. (2014) reported clear evidence that tidal oscillations in water level at the reef can lead to tidal oscillations in setup as measured at the shore. Even though the tide at Minamitorishima is small, it appears likely that a similar tide-setup interaction is occurring. With annual variability in offshore swell, the interaction leads to a strong annual oscillation in the measured amplitudes of both M_2 and K_1 tides. Offshore altimetry detects no comparable seasonality in the tide. Although the time series at the new location is again too short to yield definitive results, we can report that the tide amplitudes are substantially larger at the new location. They are in closer agreement with the tides extracted from altimetry. This is consistent with the idea that the tides as measured at the shore are no longer being suppressed by tidal variations in wave setup.

Appendix A: Consistency of altimeter and tide-gauge data processing

The source of the satellite altimeter sea-level data used in this work is the Data Unification and Altimeter Combination System (DUACS) delayed-time (DT-2018) product, described by Taburet et al. (2019). These are gridded sea-surface height anomalies, produced daily on a 0.25° global grid and based on multiple satellite missions.

The tide gauge data are in the form of daily means, formed after hourly data were subjected to an anti-aliasing low-pass filter with cutoff about 60 hours. When these data were used in comparison with altimetry, as in Figs. 2 and 7, the daily mean values were subjected to additional low-pass filtering to account for the temporal smoothing used in the DUACS solutions. The DUACS gridding algorithm used temporal correlation scales ranging from 10 to 33 days, depending on latitude (Pujol et al. 2016); at the latitude of Minamitorishima the correlation scale was approximately 29 days, so our tide-gauge filter had approximately that cutoff. However, when used in the wave-setup analysis of Sects. 4–5, the daily means were not further filtered as the goal was to capture relatively high-frequency setup anomalies.

In all accounts, it is necessary to ensure that the tide gauge data be processed in a manner as consistent as possible with the processing of the altimetry. Thus, the tide gauge data were "corrected" for long-period tides (periods between one week and 18.6 y) and the pole tide (dominant periods at 12 and 14 months). In both cases, only the ocean components were removed from the gauge data, whereas the altimetry required both ocean and solid-earth components. The altimeter data had also been adjusted by the ocean model of Carrère et al. (2016), which is a simple isostatic inverted-barometer response to pressure loading at periods longer than 20 days and a dynamic response to both winds and pressures at shorter periods. Since the Nyquist period of Topex and Jason sampling is 20 days, the idea behind the dynamic modeling is to act as a de-aliasing correction. We subsequently used the same model to remove these effects from the tide gauge data. In principle, the tide gauge data should also be adjusted for vertical land motion, but we ignored this because the motion is thought to be small, less than 0.5 mm year^{-1} based on the island GNSS data (see Appendix B).

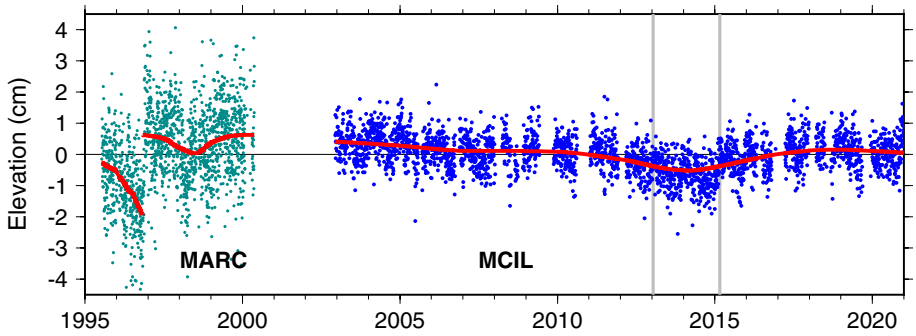

Fig. 12 Daily vertical elevations from two GNSS stations at Minamitorishima, as determined by Blewitt et al. (2018). The time series from each receiver has been demeaned. Heavy red lines are the result of a loess smoother applied to the daily data, with the break in late 1996 subjectively chosen. Grey vertical lines mark times of equipment change for the MCIL station. The MARC station employed older, now obsolete, equipment, which likely contributes to the much larger scatter

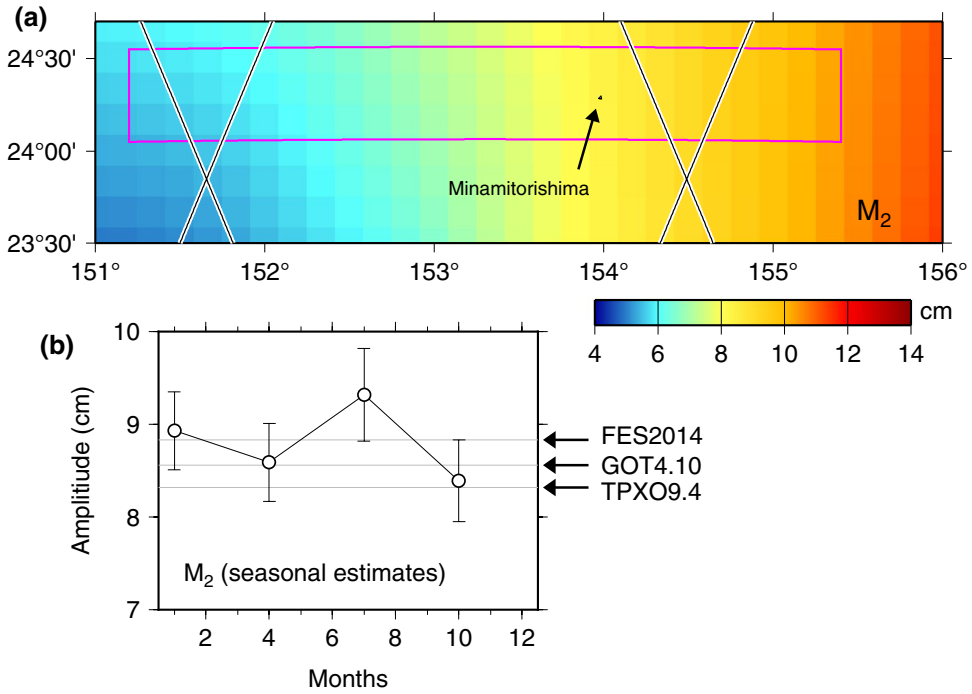

Fig. 13 **a** Ground tracks of the Topex-Jason satellites near Minamitorishima, shown over a color background of the M_2 tidal amplitudes according to global model TPXO9.4 (S. Y. Erofeeva, personal communication). **b** Mean quarterly estimates of the M_2 tide derived from all Topex-Jason data falling within the magenta box of the top panel. The tide and its spatial gradients were computed, with the latter used to interpolate to the island location. At right are the amplitudes from several widely-used global models, showing generally consistent agreement and larger than the mean tide reported at the tide gauge at its old position (Fig. 10)

Appendix B: Vertical land motion at Minamitorishima

Global Navigation Satellite System (GNSS) data have been collected on the island since 1995. In the international GNSS archives there are two stations, MARC and MCIL, from nearly identical locations (24.2901°N, 153.9787°E). The older MARC time series is short and relatively noisy. Daily estimates of vertical position as extracted by Blewitt et al. (2018) from both stations are shown in Fig. 12.

Our final time series of altimeter and tide-gauge differences (Fig. 7, lower panel) is a proxy measure for vertical position of the tide gauge (e.g. Cazenave et al. 1999). The altimeter-gauge differences are somewhat erratic during the first few years of the record, which (aside from many other errors) could be explainable by anomalous ground motion. However, the GNSS series at MARC is too noisy to shed light on the question.

The vertical rate as implied by the MCIL data is -0.39 ± 0.52 mm year^{-1}. The corresponding rate from the altimeter-gauge differences of Fig. 7 is 0.95 ± 1.0 mm year^{-1}. The uncertainty takes account of serial correlation in the time series. Within the given uncertainties the GNSS and altimeter-gauge rates are consistent even though of different sign; both overlap with zero motion. Together, they suggest the island motion has been small over the period since 1997.

Appendix C: Altimeter estimates of seasonal M_2 changes

It is desirable to know how the tide as observed at Minamitorishima (Fig. 10) compares with the tide in the surrounding deep water. Altimetry can determine this, but some care is required owing to the lack of nearby satellite tracks and the inherent aliasing problems of altimetry.

Figure 13 shows four sets of repeat tracks on the primary Topex/Poseidon-Jason orbit. Estimation of subseasonal M_2 coefficients at the one track closest to the island yields rather noisy estimates, so we have used data from all four tracks. Combining data within the magenta rectangular region of the figure, we have estimated the mean tide and its spatial gradients, and used the latter to determine the tide at the island location. (This approach works so long as there is little curvature over the region; according to the tide chart plotted in the figure background, that is here the case.) Mean monthly M_2 estimates (as could be done at the tide gauge—Fig. 10) were again rather noisy, so we solved for mean quarterly (i.e., 3-month) tides. Resulting M_2 amplitudes are shown in Fig. 13b. There is no seasonal change comparable to the ~20% seasonal range seen at the tide gauge, and certainly no large amplitude drop during winter months when the tide gauge gave amplitudes less than 7.5 cm. Only the tide-gauge estimates for the summer months are comparable to the altimetric tide.

Acknowledgements We thank Gary Mitchum and Janet Becker for useful discussions. The tide gauge at Minamitorishima is operated by the Japan Meteorological Agency, Minato City, Tokyo. The agency kindly provided us useful information about the tide gauge instrument and its relocation. The daily data were downloaded from the University of Hawaii Sea Level Center. ECMWF data were obtained from https://cds.climate.copernicus.eu. This work was partially supported by the U.S. National Aeronautics and Space Administration through the Sea Level Change and Sentinel-6 programs and by the U.S. Army Corps of Engineers (W912HZ192).

Data Availability DUACS altimeter data are available from the Copernicus Marine Service https://marine.copernicus.eu. The ECMWF ERA5 wave data are available from the Copernicus Climate Change Service https://cds.climate.copernicus.eu. Tide gauge data are available from the University of Hawaii Sea Level Center https://uhslc.soest.hawaii.edu.

References

Aucan J, Hoeke R, Merrifield MA (2012) Wave-driven sea level anomalies a the Midway tide gauge as an index of North Pacific storminess over the past 60 years. Geophys Res Lett 39:17. https://doi.org/10.1029/2012GL052993

Becker JM, Merrifield MA, Ford M (2014) Water level effects on breaking wave setup for Pacific Island fringing reefs. J Geophys Res Oceans 119:914–935. https://doi.org/10.1002/2013JC009373

Bidlot JR (2016) Ocean wave model output parameters, ECMWF Report. https://confluence.ecmwf.int/download/attachments/59774192/wave_parameters.pdf. Accessed 22 Feb 2022

Blewitt G, Hammond WC, Kreemer C (2018) Harnessing the GPS data explosion for interdisciplinary science. EOS 99. https://doi.org/10.1029/2018EO104623

Carrère L, Faugère Y, Ablain M (2016) Major improvement of altimetry sea level estimations using pressure-derived corrections based on ERA-Interim atmospheric reanalysis. Ocean Sci 12:825–842. https://doi.org/10.5194/os-12-825-2016

Cazenave A, Dominh K, Ponchaut F, Soudarin L, Cretaux JF, Le Provost C (1999) Sea level changes from Topex-Poseidon altimetry and tide gauges, and vertical crustal motions from DORIS. Geophys Res Lett 26:2077–2080

Cheney R, Miller L, Agreen R, Doyle N, Lillibridge J (1994) TOPEX/POSEIDON: the 2-cm solution. J Geophys Res Oceans 99:24555–24563

Cheriton OM, Storlazzi CD, Rosenberger KJ (2016) Observations of wave transformation over a fringing coral reef and the importance of low-frequency waves and offshore water levels to runup, overwash, and coastal flooding. J Geophys Res Oceans 121:3121–3140. https://doi.org/10.1002/2015JC011231

Dodet G, Melet A, Ardhuin F, Bertin X, Idier D, Almar R (2019) The contribution of wind-generated waves to coastal sea-level changes. Surv Geophys 40:1563–1601. https://doi.org/10.1007/s10712-019-09557-5

Gourlay MR (1996) Wave set-up on coral reefs. 2. Set-up on reefs with various profiles. Coast Eng 28:17–55

Hersbach H et al (2020) The ERA5 global reanalysis. Q J R Met Soc 146:1999–2049. https://doi.org/10.1002/qj.3803

Hoeke RK, McInnes KL, Kruger JC, McNaught RJ, Junter JR, Smithers SG (2013) Widespread inundation of Pacific islands triggered by distant-source wind-waves. Glob Planet Change 108:128–138. https://doi.org/10.1016/j.gloplacha.2013.06.006

Holman RA, Sallenger AH (1985) Setup and swash on a natural beach. J Geophys Res 90:945–953

Longuet-Higgins MS, Stewart RW (1962) Radiation stress and mass transport in gravity waves, with application to surf-beats. J Fluid Mech 13:481–504

Lugo-Fernández A, Roberts HH, Wiseman WJ (1998) Tide effects on wave attenuation and wave set-up on a Caribbean coral reef. Estuar Coast Shelf Sci 47:385–393

Merrifield MA, Becker JM, Ford M, Yao Y (2014) Observations and estimates of wave-driven water level extremes at the Marshall Islands. Geophys Res Lett 41:7245–7253. https://doi.org/10.1002/2014GL061005

Mitchum GT (1998) Monitoring the stability of satellite altimeters with tide gauges. J Atmos Ocean Tech 15:721–730

Monismith SG (2007) Hydrodynamics of coral reefs. Ann Rev Fluid Mech 39:37–55. https://doi.org/10.1146/annurev.fluid.38.050304.092125

Monismith SG, Herdman LMM, Ahmerkamp S, Hench JL (2013) Wave transformation and wave-driven flow across a steep coral reef. J Phys Oceanogr 43:1356–1379. https://doi.org/10.1175/JPO-D-12-0164.1

Munk WH, Sargent MC (1948) Adjustment of Bikini Atoll to ocean waves. Trans Am Geophys Union 29:855–860 (reprinted in Geological Survey Prof. Paper 260-C, U. S. Govt. Printing Off., Washington, 1954)

Pomeroy A, Lowe R, Symonds G, Van Dongeren A, Moore C (2012) The dynamics of infragravity wave transformation over a fringing reef. J Geophys Res Oceans 117:C11022. https://doi.org/10.1029/2012JC008310

Pujol MI, Faugère Y, Tauburet G, Dupuy S, Pelloquin C, Ablain M, Picot N (2016) DUACS DT2014: the new multi-mission

altimeter data set reprocessed over 20 years. Ocean Sci 12:1067–1090. https://doi.org/10.5194/os-12-1067-2016
Raubenheimer B, Guza RT, Elgar S (1996) Wave transformation across the inner surf zone. J Geophys Res 101:25589–25597
Ray RD, Beckley BD, Lemoine FG (2010) Vertical crustal motion derived from satellite altimetry and tide gauges, and comparisons with DORIS. Adv Space Res 45:1510–1522. https://doi.org/10.1016/j.asr.2010.02.020
Ray RD, Loomis BD, Zlotnicki V (2021) The mean seasonal cycle in relative sea level from satellite altimetry and gravimetry. J Geod 95:80. https://doi.org/10.1007/s00190-021-01529-1
Taburet G, Sanchez-Roman A, Ballarotta M, Pujol MI, Legeais JF, Fournier F, Faugère Y, Dibarboure G (2019) DUACS DT2018: 25 years of reprocessed sea level altimetry products. Ocean Sci 15:1207–1224. https://doi.org/10.5194/os-15-1207-2019
Tran N, Labroue S, Philipps S, Bonner E, Picot N (2010) Overview and update of the sea state bias corrections for the Jason-2, Jason-1 and TOPEX missions. Mar Geod 33:348–362
Vetter O, Becker JM, Merrifield MA, Pequignet AC, Aucan J, Boc SJ, Pollock CE (2010) Wave setup over a Pacific Island fringing reef. J Geophys Res 115:C12066. https://doi.org/10.1029/2010JC006455
Vinogradov SV, Ponte RM (2010) Annual cycle in coastal sea level from tide gauges and altimetry. J Geophys Res 115:C04021. https://doi.org/10.1029/2009JC005767
Vinogradov SV, Ponte RM (2011) Low-frequency variability in coastal sea level from tide gauges and altimetry. J Geophys Res 116:C07006. https://doi.org/10.1029/2011JC007034
Walsh EJ, Jackson FC, Uliana E, Swift RN (1989) Observations on electromagnetic bias in radar altimeter sea surface measurements. J Geophys Res 94:14575–14584
Williams J, Hughes CW (2013) The coherence of small island sea level with the wider ocean: a model study. Ocean Sci 9:111–119. https://doi.org/10.5194/os-9-111-2013
Woodworth PL (2020) Wave setup at Tristan de Cunha. Afr J Mar Sci 42:233–245. https://doi.org/10.2989/1814232X.2020.1776390
Woodworth PL et al (2019) Factors affecting sea level changes at the coast. Surv Geophys 40:1351–1397. https://doi.org/10.1007/s10712-019-09531-1
Zemunik P, Šepić J, Pellikka H, Ćatipović L, Vilibić I (2021) Minute sea-level analysis (MISELA): a high-frequency sea-level analysis global dataset. Earth Syst Sci Data 13:4121–4132. https://doi.org/10.5194/essd-13-4121-2021